RadioGraphics

Spectrum of Multilocular Cystic Hepatic Lesions: CT and MR Imaging Findings with Pathologic Correlation[1]

Li Jun Qian, MD • Jiong Zhu, MD • Zhi Guo Zhuang, MD • Qiang Xia, MD • Qiang Liu, MD • Jian Rong Xu, MD

SA-CME

See www.rsna.org/education/search/RG

LEARNING OBJECTIVES FOR TEST 5

After completing this journal-based SA-CME activity, participants will be able to:

- Describe the wide spectrum of common and uncommon multilocular cystic hepatic lesions.
- Recognize the features of these lesions on CT and MR images and correlate these features with pathologic findings.
- Identify the crucial points for differential diagnosis among lesions with similar image patterns.

TEACHING POINTS

See last page

A multilocular cystic hepatic lesion detected at computed tomography (CT) and magnetic resonance (MR) imaging is a common but nonspecific radiologic finding that can cause potential challenges for differential diagnosis. This imaging pattern may be observed in a wide spectrum of common and uncommon neoplastic or nonneoplastic entities. Neoplastic lesions include cystadenoma, cystadenocarcinoma, hepatocellular carcinoma (HCC), metastases, mesenchymal hamartoma, and inflammatory myofibroblastic tumor. Nonneoplastic lesions include hepatic abscess, echinococcal cyst, intrahepatic hematoma, and biloma. The multiple coalescent cysts seen in polycystic liver disease may exhibit an imaging pattern similar to that of a multilocular cystic lesion. Mural nodularity, irregular thickness of the septa, ragged inner surface, and typical enhancement pattern in the solid portion of the lesion are often indicative of malignancy, although multilocular primary or secondary malignant tumors are uncommon. Recognition of the more common necrosis or cystic change of HCC and metastases induced by locoregional or systemic treatment also is important. The nonenhanced cystic component may be composed of different types of fluids (eg, serous, mucinous, proteinaceous, hemorrhagic, bilious, or mixed) or spontaneous or treatment-related necrosis, whereas the septa may be formed by a wide range of tissues depending on the lesion type. An understanding of the CT and MR imaging findings of these lesions and their respective pathologic correlation aids in accurate diagnosis.

Introduction

Hepatic lesions with a multilocular cystic appearance are frequently encountered in routine radiologic practices. This imaging pattern covers a wide spectrum of common and uncommon entities. A cystic lesion is a well-defined lesion with predominant near-water attenuation (0–30 HU) or signal intensity that exhibits negligible enhancement at dynamic imaging; the attenuation or signal intensity can be slightly different from that of pure water because of the diversity in fluid composition. The

Teaching Point

Abbreviations: ADPKD = autosomal dominant polycystic kidney disease, ADPLD = autosomal dominant PLD, CECT = contrast-enhanced CT, GIST = gastrointestinal stromal tumor, HCC = hepatocellular carcinoma, H-E = hematoxylin-eosin, IMT = inflammatory myofibroblastic tumor, PLD = polycystic liver disease, RFA = radiofrequency ablation, TACE = transarterial chemoembolization

RadioGraphics 2013; 33:1419–1433 • **Published online** 10.1148/rg.335125063 • **Content Codes:** CT GI MR

[1]From the Departments of Radiology (L.J.Q., J.Z., Z.G.Z., J.R.X.), Hepatic Surgery (Q.X.), and Pathology (Q.L.), Renji Hospital, Shanghai Jiaotong University School of Medicine, No. 1630 Dongfang Rd, Pudong, Shanghai 200127, P.R. China. Presented as an education exhibit at the 2011 RSNA Annual Meeting. Received April 11, 2012; revision requested May 9 and received September 25; accepted January 28, 2013. For this journal-based SA-CME activity, J.R.X. has disclosed financial relationships (see p 1432); the other authors, editor, and reviewers have no relevant relationships to disclose. Supported in part by the Shanghai Leading Academic Discipline Project (S30203) and the Scientific Program of Shanghai Jiaotong University School of Medicine (YZ1004). **Address correspondence to** J.R.X. (e-mail: *xujianr@gmail.com*).

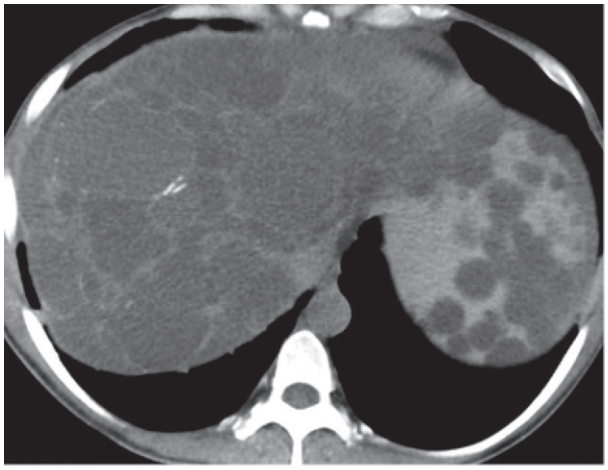

a.

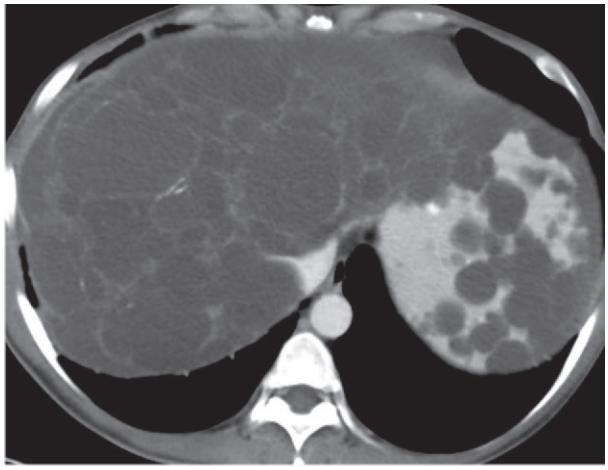

b.

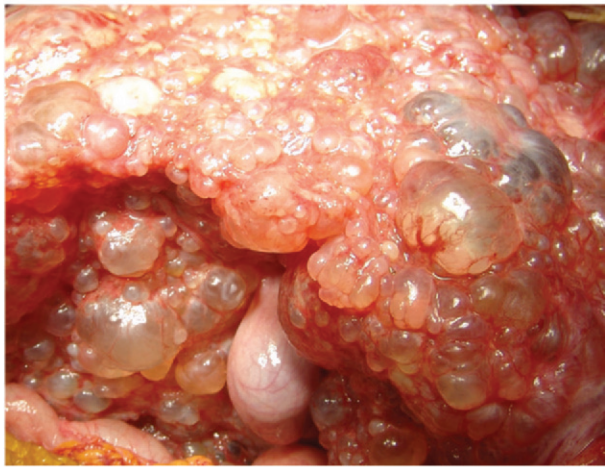

c.

Figure 1. Polycystic liver disease in a 42-year-old woman who underwent liver transplantation. Preoperative unenhanced CT **(a)** and portal venous phase contrast-enhanced CT (CECT) **(b)** images show multiple thin-walled coalescent cysts with regular margins. Calcifications can be observed within the walls of several cysts. **(c)** Intraoperative photograph shows numerous translucent cysts that have extensively replaced the hepatic parenchyma.

internal septa are defined as the partitions or membranes that divide the lesion into multiple compartments. Septa may vary in thickness, uniformity, extent of enhancement, and mural nodularity.

Both the cystic components and the internal septa found in imaging studies reflect the underlying pathologic alterations. Generally, the cystic component may be secondary to *(a)* liquid substances, including serous, mucinous, bilious, hemorrhagic, proteinaceous, or mixed fluids; *(b)* intratumoral necrosis; or *(c)* tissue with a high water content. The septa may contain a wide range of tissues, including epithelium, fibrotic tissue, stroma, neoplastic tissue, and inflammatory cells, depending on the lesion type. The purpose of this article is to review the wide spectrum of multilocular cystic hepatic lesions found at computed tomography (CT) and magnetic resonance (MR) imaging and to discuss the correlated pathologic features.

Teaching Point

Congenital Lesion: Polycystic Liver Disease

Polycystic liver disease (PLD) is a congenital disorder commonly associated with autosomal dominant polycystic kidney disease (ADPKD). However, patients with autosomal dominant PLD (ADPLD) may not have the accompanying ADPKD (1). ADPKD with hepatic involvement and ADPLD are genetically different but pathologically indistinguishable diseases. In patients with PLD, the liver usually is enlarged with multiple, diffusive, innumerable cysts of various sizes. Compression of the adjacent organs and major intrahepatic vasculatures is common because of the mass effect of hepatomegaly.

At imaging, patients with PLD may show a multilocular-appearing lesion composed of multiple coalescent cysts, but the lesion is not a true multilocular cystic lesion. The cysts contain clear or yellow fluid. Their attenuation and signal intensity are similar to those of water at CT and MR imaging, respectively. The cystic wall is very thin and regular without enhancement. Increased attenuation at nonenhanced CT or increased T1-weighted signal intensity at MR imaging may suggest hemorrhage or infection. Calcifications in the cyst wall indicate prior hemorrhage or infection (Fig 1).

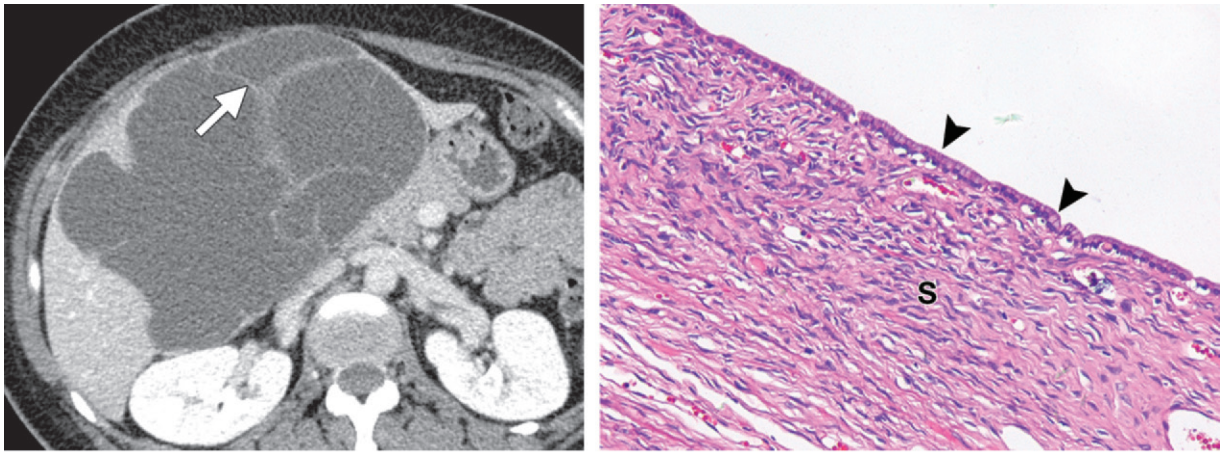

a. b.

Figure 2. Biliary cystadenoma in a 42-year-old woman. **(a)** Thin-section portal venous phase CECT image shows a large cystic hepatic lesion with a multilocular appearance and enhancing internal septa (arrow). **(b)** Photomicrograph (original magnification, ×100; hematoxylin-eosin [H-E] stain) shows a single layer of epithelial cells (arrowheads) lining the inner cystic space and covering the compact ovarian-like stroma *(S)*.

Neoplasms

Biliary Cystadenoma and Cystadenocarcinoma

Biliary cystadenomas and cystadenocarcinomas are rare neoplasms of the biliary system. Approximately 85% of cases appear in the intrahepatic bile duct; the others occur within the extrahepatic biliary tree or gallbladder (2). The clinical manifestations of these neoplasms are variable and nonspecific. Biliary cystadenomas occur predominantly in middle-aged female patients and may potentially transform into cystadenocarcinomas. As a result, complete surgical excision is required.

At CT and MR imaging, a typical biliary cystadenoma or cystadenocarcinoma appears as a large, solitary, multilocular cystic lesion with well-circumscribed smooth margins and internal septa. Enhancement is commonly seen along the wall and internal septa (Fig 2). Calcification may be seen within the wall and the septa in a minority of cases. Although the presence of hemorrhagic internal fluid, a solid mural nodule, or coarse calcification along the wall or septa is more commonly associated with cystadenocarcinoma, differentiation between cystadenocarcinoma and cystadenoma is often difficult when based solely on imaging findings because of the significant overlap in radiologic features (2).

At gross inspection, biliary cystadenomas and cystadenocarcinomas are cystic masses with multiple locules lined by septa with or without nodules and soft-tissue masses. The locules contain clear to turbid fluid, which may be mucinous or, less frequently, serous, mixed, hemorrhagic, or biliary. Viewed microscopically, the septa in biliary cystadenomas typically are composed of columnar, but seldom cuboidal, flattened, and rarely papillary epithelia that overlie the subepithelial mesenchymal stroma. A highly cellular mesenchymal tissue that resembles the ovarian stroma (ovarian-like stroma) occurs in over 80% of cases. This type of stroma is reported to have been found exclusively in female patients.

In recent studies, the positive immunohistochemical detection of estrogen and progesterone receptors in the ovarian-like stroma suggests that sex-related hormones may play an important role in tumor pathogenesis (3,4). In biliary cystadenocarcinomas, the ovarian-like stroma observed in female patients indicates that the tumor may have originated from a preexisting cystadenoma. Tumors found in male patients may be irrelevant in terms of pathogenesis from cystadenoma because they do not have this type of stroma. Large polypoid, papillary excrescences in the wall usually indicate malignant transformation. In biliary cystadenocarcinomas, the malignant portion may consist of hyperchromatic columnar cells that form irregular papillary, tubular, squamous, spindled, or mixed projections into the cyst lumen (5).

Hepatocellular Carcinoma

Hepatocellular carcinoma (HCC) with heterogeneous internal architecture (mosaic-patterned HCC) may undergo varying degrees of spontaneous intratumoral necrosis or hemorrhage. The area of necrosis or hemorrhage may be extensive, such that the HCC lesion could manifest as an atypical multilocular cystic mass (Figs 3, 4) (6).

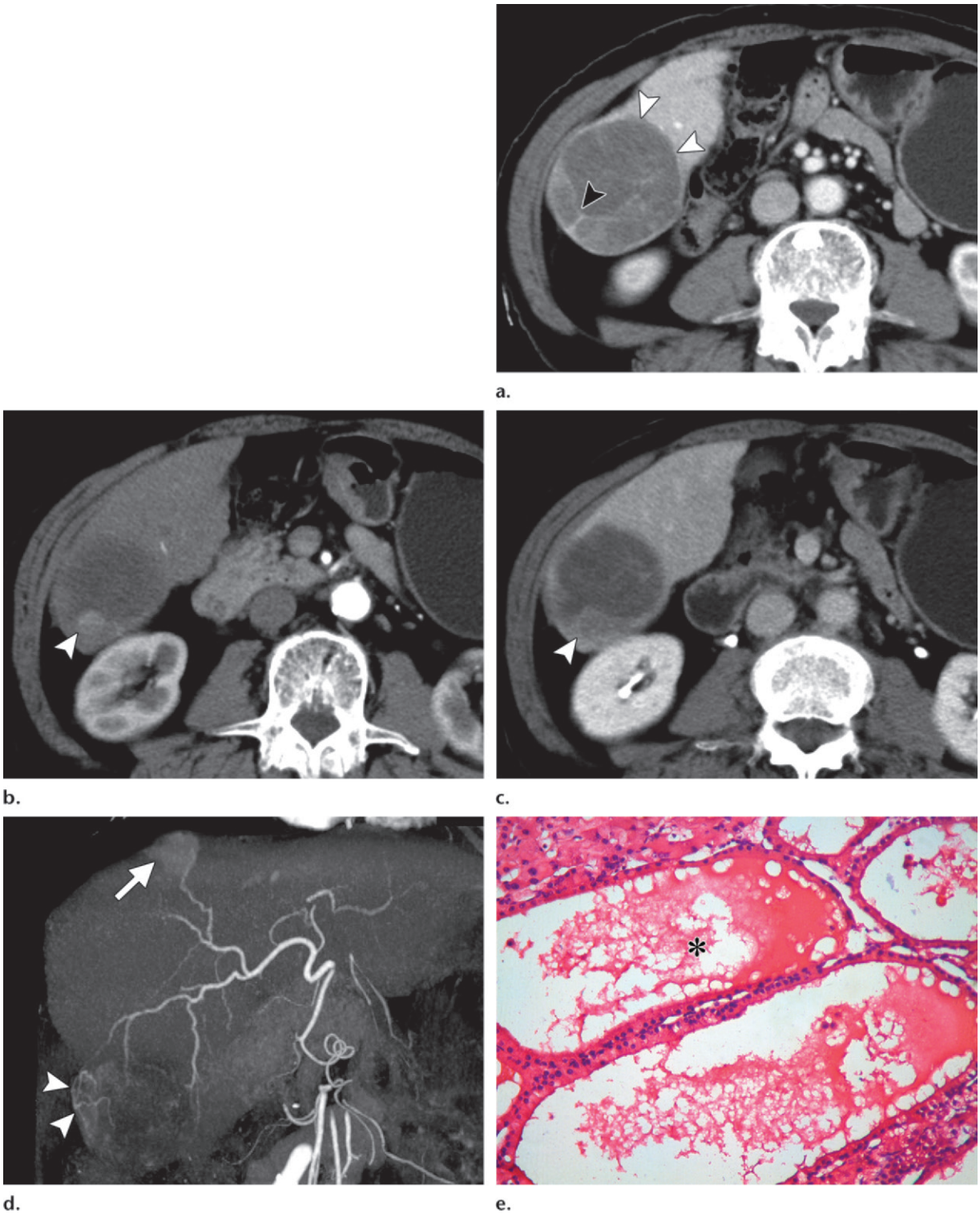

Figure 3. Multifocal HCCs in a 65-year-old woman with a history of hepatitis B–related liver cirrhosis. The tumors did not undergo any prior treatment. **(a)** Portal venous phase CECT image shows a multilocular mass (white arrowheads) in segment VI, with cystic attenuation and enhancing septa (black arrowhead). **(b, c)** Arterial **(b)** and delayed phase **(c)** CECT images superior to **a** show a solid mural nodule (arrowhead) with the classic HCC hemodynamics of arterial enhancement and late contrast material washout. **(d)** Arterial maximum intensity projection image shows the visible internal vessels with irregular, distorted contours (arrowheads) within the mass, findings that strongly indicate HCC. A typical hypervascular HCC nodule in segment VIII (arrow) is also noted. **(e)** Photomicrograph (original magnification, ×100; H-E stain) of the lesion in segment VI shows HCC cells arranged in a cystically dilated pseudoglandular pattern (*).

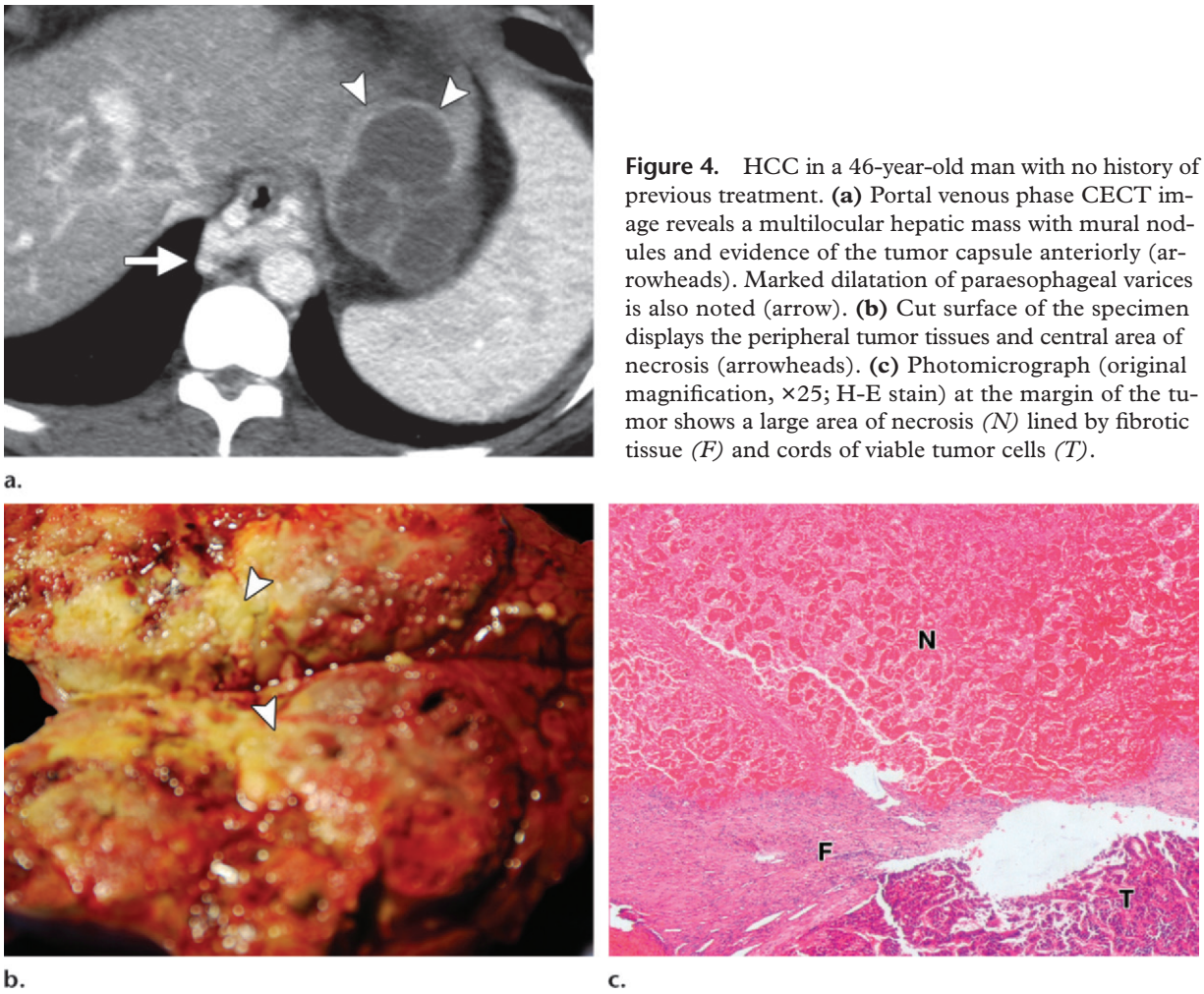

Figure 4. HCC in a 46-year-old man with no history of previous treatment. **(a)** Portal venous phase CECT image reveals a multilocular hepatic mass with mural nodules and evidence of the tumor capsule anteriorly (arrowheads). Marked dilatation of paraesophageal varices is also noted (arrow). **(b)** Cut surface of the specimen displays the peripheral tumor tissues and central area of necrosis (arrowheads). **(c)** Photomicrograph (original magnification, ×25; H-E stain) at the margin of the tumor shows a large area of necrosis *(N)* lined by fibrotic tissue *(F)* and cords of viable tumor cells *(T)*.

The attenuation of the necrotic or hemorrhagic area is close to but slightly higher than that of pure fluid, whereas the T2-weighted signal intensity is lower. Hemorrhage in HCC tends to be more microscopic than in hepatic adenomas, where hemorrhage is more macroscopic.

Enhancing mural nodules that microscopically correspond to viable tumor components provide reliable evidence of malignancy. The mural nodules in multilocular cystic HCC that correspond to viable tumor components may demonstrate the classic HCC hemodynamics of arterial enhancement and late contrast material washout at both CECT and MR imaging (7). This feature is critical in differentiating HCC from other cystic neoplasms. Furthermore, if "abnormal internal vessels or a variegated pattern" is observed in mural nodules, it may strongly indicate HCC. Abnormal internal vessels or a variegated pattern is defined by Nino-Murcia et al (8) as either visible internal vessels with an irregular distorted contour or randomly distributed hyperattenuating and hypoattenuating regions found in a focal hepatic mass. The appearance of this pattern suggests HCC with a 90% positive predictive value and 98% specificity (Fig 3).

Teaching Point

Use of the delayed phase is helpful in presenting prolonged enhancement of the capsules and septa (Fig 4). In different studies, thin-rim-enhancing capsules have been observed in 10%–78% of HCC lesions (9). However, capsules are not specific for HCC because they also occur in hepatic adenomas (10). The thin-rim-enhancing capsules in HCC are typically thin and discontinuous and consist of peritumoral sinusoids and fibrosis (9,11). The discontinuity of tumor capsules is likely associated with early microvascular invasion and postoperative recurrence. Internal septa are histopathologically similar to the capsules because they may result from the incorporation of separate nodules into a single, large, mosaic-patterned HCC mass as the nodules grow and aggregate (6).

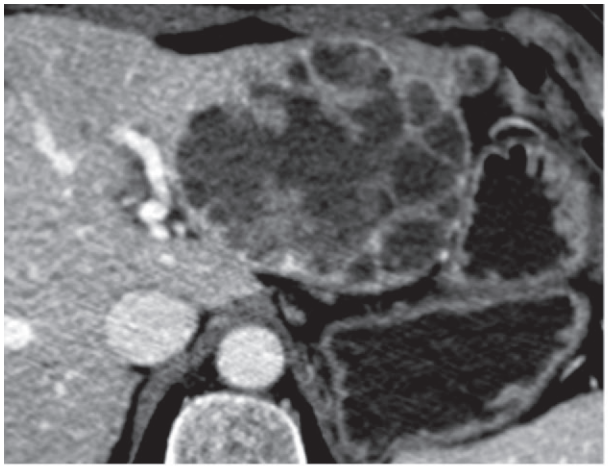

5a.

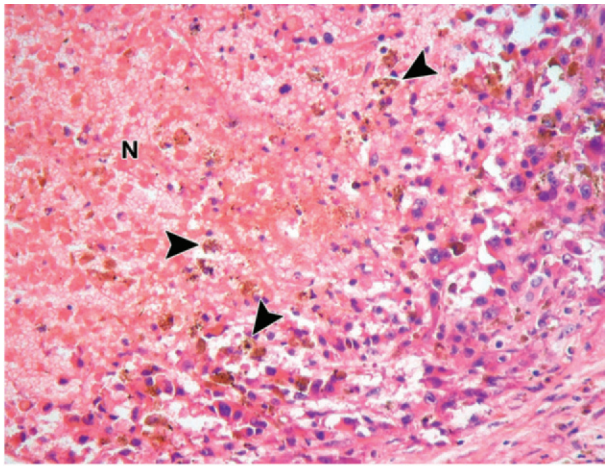

5b.

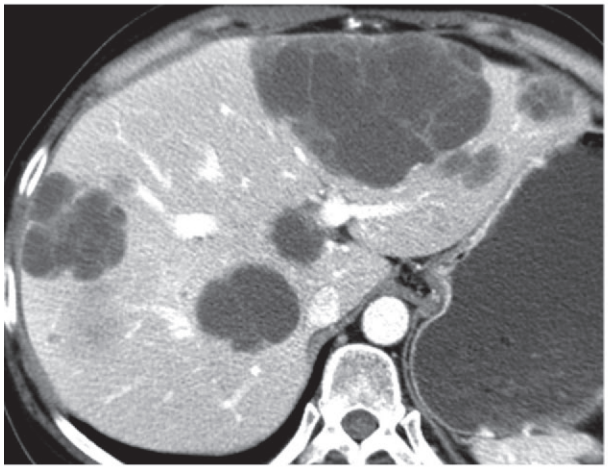

6a.

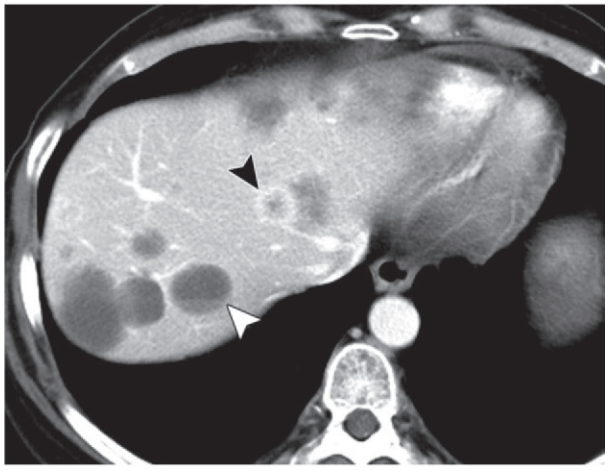

6b.

Figures 5, 6. **(5)** Metastatic melanoma in a 58-year-old woman. **(a)** Portal venous phase CECT image shows a multilocular cystic hepatic lesion in the left lobe with enhancing internal septa and mural nodules. **(b)** Photomicrograph (original magnification, ×100; H-E stain) at the periphery of the mass shows an extensive area of intratumoral necrosis *(N)* surrounded by viable tumor cells and fibrotic tissue with scattered melanin pigment (arrowheads). **(6)** Metastatic gastrinoma in the pancreas of a 39-year-old woman. **(a)** Portal venous phase CECT image shows multiple multilocular cystic masses within the liver. **(b)** CT image obtained superior to **a** demonstrates a hypervascular solid nodule without obvious cystic change (black arrowhead). A fluid-fluid level is also present within another cystic lesion (white arrowhead), a finding indicative of intratumoral hemorrhage.

Noticeably, liver cirrhosis is associated with a markedly increased risk of HCC that is highest among patients with hepatitis B or hepatitis C. A mass in the cirrhotic liver should always be considered to be HCC until proved otherwise.

Locoregional therapy, including percutaneous radiofrequency ablation (RFA) and transarterial chemoembolization (TACE), is recommended and is widely performed to control HCC (12). Both RFA and TACE are common sources of treatment-related necrosis. Compared with spontaneous necrosis, the coagulative necrosis in the ablative zone that is induced by RFA appears oval, round, or tubular, with typical high or mixed high signal intensity on T1-weighted MR images and homogeneously low signal intensity on T2-weighted MR images (13). TACE-induced hemorrhagic coagulative necrosis is characterized by hyperattenuating iodized oil retention within the tumor at CT. Hepatic capsular retraction is common in patients who have undergone RFA or TACE, a finding that may prompt the possibility of prior treatment (14).

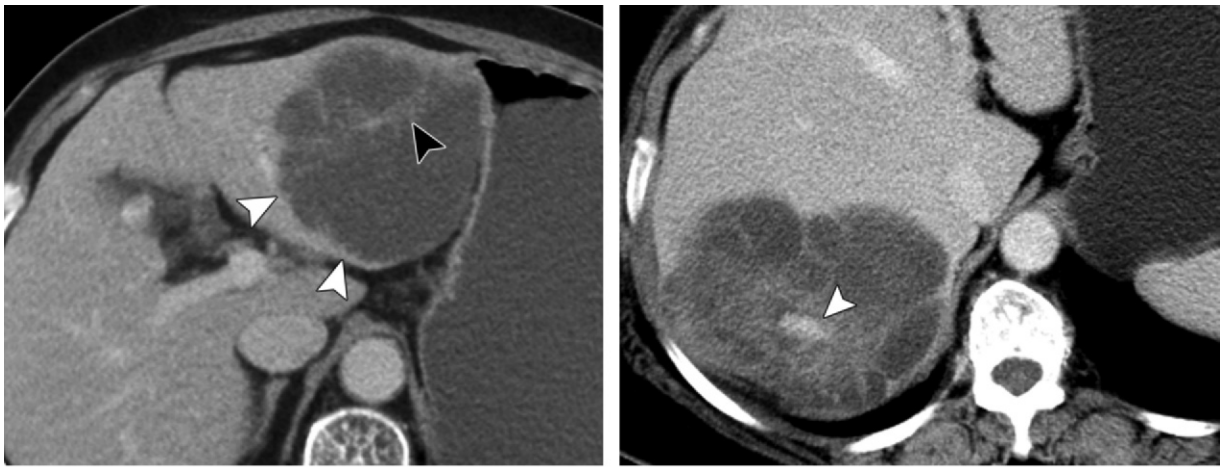

7. 8.

Figures 7, 8. **(7)** Cystic metastatic rectal cancer in a 74-year-old woman. Equilibrium phase CECT image shows the ragged inner surface (white arrowheads) of the mass and the irregular internal enhancing septa (black arrowhead). **(8)** Cystic liver metastasis that originated from an ovarian granulosa cell tumor in a 62-year-old patient. Equilibrium phase CECT image depicts a multilocular cystic lesion with enhancement of the septa and solid portions (arrowhead) in the center.

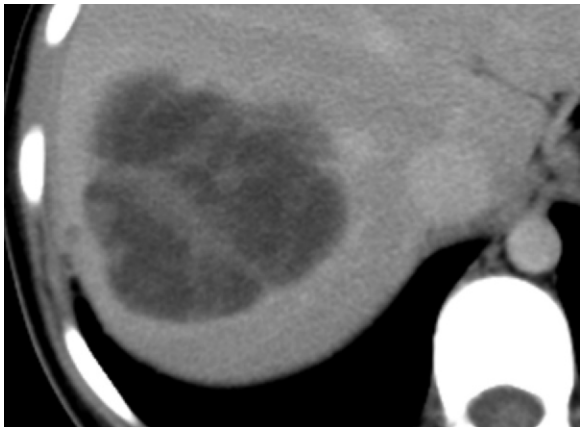

Figure 9. Metastatic GIST treated with imatinib mesylate in a 17-year-old woman. Equilibrium phase CECT image shows a cystic mass with internal septa of varied thicknesses and multiple mural nodules.

Metastases

Metastatic neoplasms are the most common malignant tumor of the liver and are far more common than primary liver neoplasms. Adenocarcinomas are the most frequent type, followed by squamous cell carcinomas; neuroendocrine carcinomas; and, rarely, melanomas, lymphomas, and sarcomas. In general, most hepatic metastases are hypovascular. However, liver metastases from thyroid carcinomas, pancreatic neuroendocrine tumors, malignant melanomas, and carcinoids are typically hypervascular (15).

Metastases predominantly composed of large intratumoral areas of liquid attenuation with negligible contrast enhancement throughout the contrast phases are regarded as cystic metastases, which are far less common than hypovascular and hypervascular metastases. Cystic metastases can be formed through *(a)* necrosis of hypervascular metastases secondary to rapid growth beyond the vascular supply, which is frequently demonstrated in metastases from a neuroendocrine tumor, melanoma, or gastrointestinal stromal tumor (GIST) (Figs 5, 6); *(b)* abundant mucin production by acinar structures and glandular tissues from mucinous adenocarcinoma, such as colorectal or ovarian carcinoma (Figs 7, 8); or *(c)* systemic or locoregional treatment (Fig 9) (16–18).

Teaching Point

Cystic metastatic lesions may appear as a multilocular cystic pattern. Compared with other benign cystic lesions, the enhancing septa in a metastatic cystic lesion, which usually represent viable tumor cells with fibrotic tissues, tend to have an irregular thickness. The inner surfaces are typically ragged, serrated, and ill-defined, with multiple mural nodules (Figs 5, 7, 9). The attenuation of the cystic component is usually higher than that of pure fluid because of the presence of necrosis, mucin, or hemorrhage. Final diagnosis of metastases is not difficult when cystic masses are diffusively or multifocally

distributed with irregular septa and enhancing mural nodules in the context of a high-risk oncologic scenario.

Varying degrees of intratumoral cystic change or necrosis may be seen in different lesions of a single case, with a spectrum of imaging findings from the pure solid hypervascular nodule to the subtotal cystic mass (Fig 6). This result may reflect different stages in the evolution of cystic metastases. However, distinguishing solitary cystic metastases from other malignant cystic neoplasms without knowledge of their primary malignancy can be problematic because the imaging finding is usually unspecific.

Treated liver metastases may also appear as multilocular cystic lesions with decreased attenuation at CT and increased signal intensity on T2-weighted images. One well-documented representative example is the cystic change in metastatic GIST after treatment with imatinib mesylate (Gleevec; Novartis Pharma, Basel, Switzerland). Almost all GISTs express a mutant form of the KIT protein (CD117 or c-kit), a tyrosine-kinase receptor, which results in abnormally activated tumor-cell proliferation. Imatinib mesylate specifically inhibits tyrosine-kinase enzymes, thereby allowing targeted control of GISTs (19). Compared with untreated lesions, treated metastatic GISTs may show varying degrees of decreased tumor density, decreased tumor enhancement, and substantial cystic change (Fig 9).

However, metastatic lesions may become paradoxically large after treatment because of extensive cystic degeneration. The increase in the necrotic component and devascularization should also be considered instead of relying solely on lesion size when assessing the treatment response (20,21). The reduced attenuation and cystic change exhibited in treated metastatic GISTs correspond to the myxoid material and, occasionally, the hemorrhage or necrosis, the attenuation of which is higher than that of pure fluid. The presence of newly developed soft-tissue nodules within the cystic component of the treated lesion strongly suggests tumor progression (22,23).

Inflammatory Myofibroblastic Tumor

Inflammatory myofibroblastic tumor (IMT), also known as inflammatory pseudotumor, is a relatively rare entity characterized by proliferation of myofibroblastic spindle cells mixed in with an inflammatory infiltrate of plasma cells, lymphocytes, and eosinophils (24). The cause of IMT is unclear. However, postinflammatory regenerative processes may be associated with the pathogenesis of the disease (25,26). IMT may manifest with nonspecific symptoms, including right upper quadrant pain, jaundice, and occasionally obliterative phlebitis. At gross examination, IMTs tend to be well circumscribed or multinodular with a fibrotic or myxoid cut surface. The surface may show a variegated appearance with focal areas of necrosis, hemorrhage, or calcification (24).

The radiologic findings for IMT are nonspecific. Commonly, the tumors are hypoattenuating to liver parenchyma on unenhanced images, and variable patterns of enhancement are observed after contrast material enhancement, including peripheral enhancement or enhancement of multiple internal septa (27). The lesion occasionally appears as a mutilobular cystic mass with multiple enhancing internal septa. Delayed enhancement of part of the lesion, including the septa, is a typical finding, presumably due to delayed washout of contrast medium accumulating in the extravascular space (28,29). Septa in IMT may represent myofibroblastic proliferation, with a variety of plasma cells, lymphocytes, neutrophils, macrophages, mast cells, and fibrotic stroma, whereas nonenhanced cystic-appearing areas reflect internal hemorrhage and necrosis (Fig 10) (29,30).

Mesenchymal Hamartoma

Mesenchymal hamartoma of the liver is a rare type of neoplasm. However, it is the second most common benign hepatic tumor in children, after infantile hemangioendothelioma. It usually occurs in male children younger than 2 years of age. The exact pathogenesis is unknown. However, several theories have been proposed, including developmental ductal plate malformation, regional hepatic lobe ischemia, toxic injury to sinusoidal fat-storing cells, an imprinting defect due to chromosomal abnormalities, and a genuine neoplastic lesion (31,32). Depending on tumor size, clinical presentation may include a palpable abdominal mass, anorexia, nausea, and vomiting. Jaundice, portal vein hypertension, and lower extremity edema may also develop because of compression of the bile duct and hepatic vein by the tumor.

The radiologic features of mesenchymal hamartoma largely depend on the predominance of cystic or solid components. At CT, mesenchymal hamartoma appears as a complex cystic mass with avascular cystic portions of fluid attenuation and stromal portions that are relatively hypovascular to the surrounding hepatic parenchyma. Enhancement of the septa and solid (stromal) elements is observed after contrast material enhancement (Fig 11) (33). At MR imaging, solid

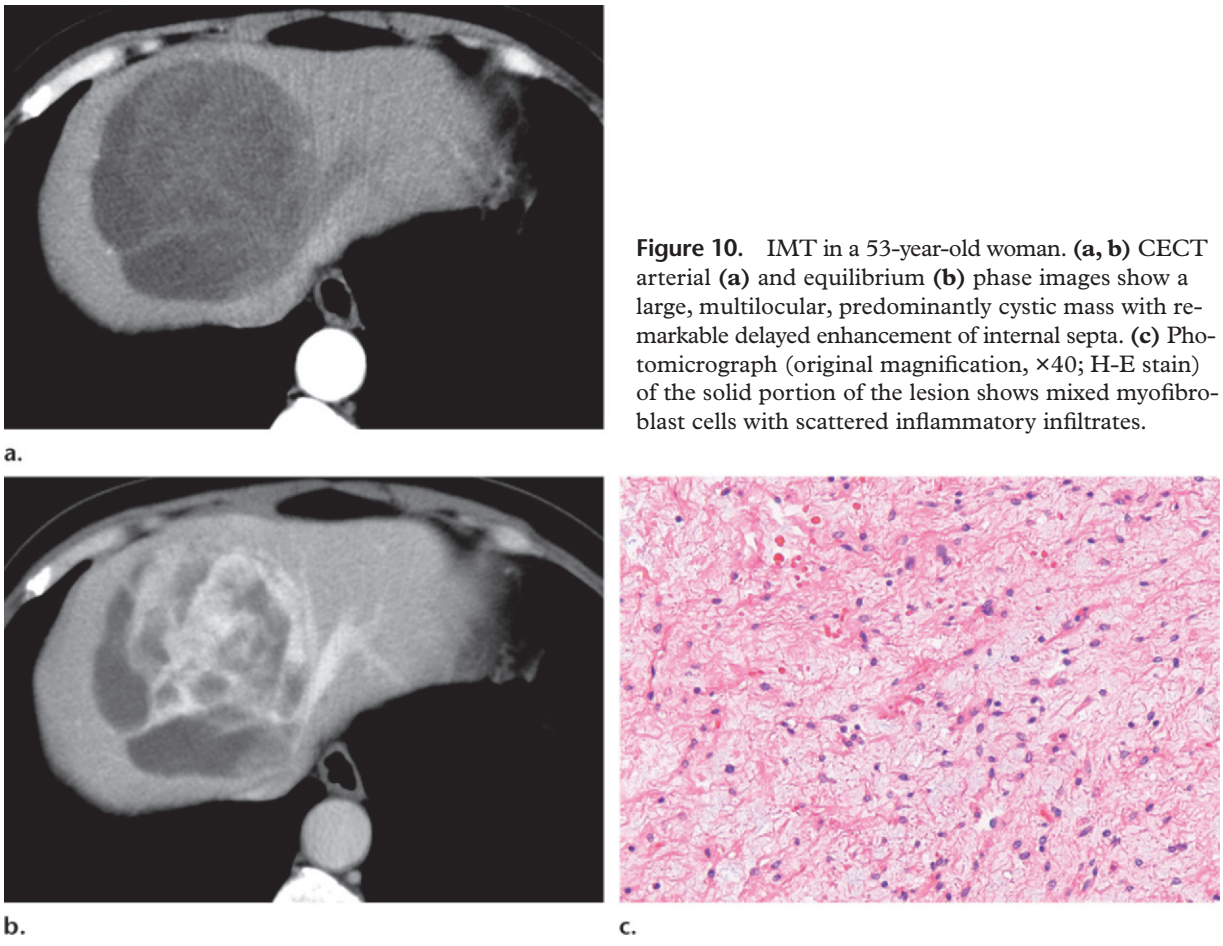

Figure 10. IMT in a 53-year-old woman. **(a, b)** CECT arterial **(a)** and equilibrium **(b)** phase images show a large, multilocular, predominantly cystic mass with remarkable delayed enhancement of internal septa. **(c)** Photomicrograph (original magnification, ×40; H-E stain) of the solid portion of the lesion shows mixed myofibroblast cells with scattered inflammatory infiltrates.

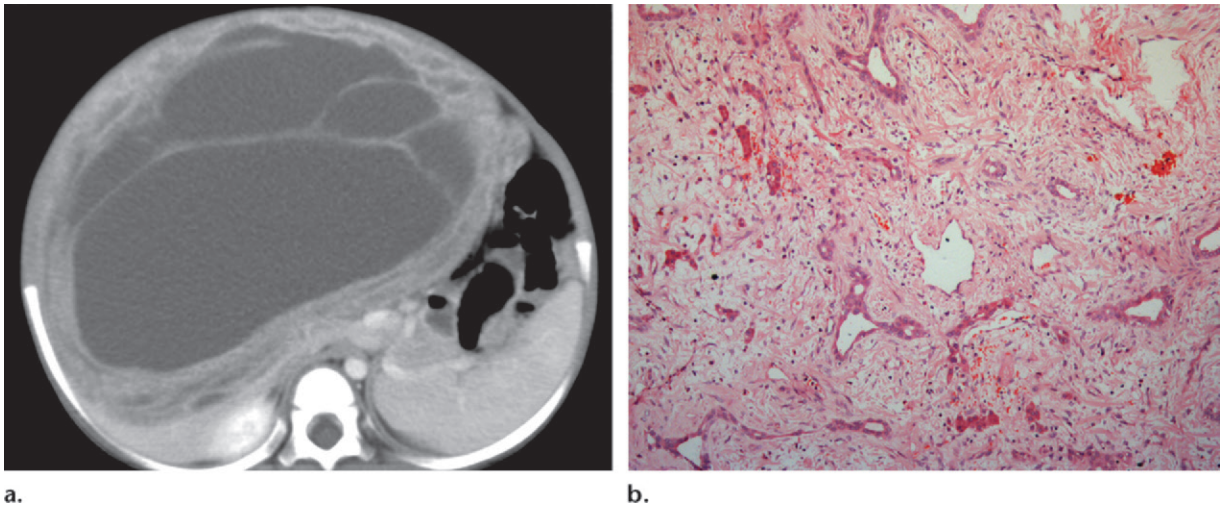

Figure 11. Mesenchymal hamartoma in a 28-month-old boy. **(a)** Portal venous phase CECT image shows a huge, multiseptated mass with mixed solid and cystic compartments and displacement of major abdominal vessels. **(b)** Photomicrograph (original magnification, ×10; H-E stain) shows the solid portion of the mass, which is characterized by abundant myxoid mesenchymal stroma and bile-duct proliferation.

portions may appear hypointense relative to the adjacent liver on both T1- and T2-weighted images because of fibrotic tissue. Cystic portions demonstrate signal intensity generally close to water signal intensity on T2-weighted images and variable signal intensity on T1-weighted images, depending on the protein content of the fluid in the cystic component.

Figure 12. Pyogenic liver abscess in a 44-year-old man. Axial postcontrast (120 seconds) CECT image delineates the double target sign, which consists of a hypoattenuating central area surrounded by an inner hyperattenuating ring (arrow) and an outer hypoattenuating zone (arrowheads), in the left hepatic lobe.

At macroscopic examination, the tumor can vary in size from a few centimeters to more than 30 cm in diameter and typically appears as a solitary tumor with both cystic and solid compartments. Cystic spaces are often filled with clear, yellow, or gelatinous fluid with serous or mucoid materials. At histologic examination, mesenchymal hamartoma typically consists of a disorganized arrangement of hepatic parenchyma, proliferated bile ducts, and mesenchymal components. The mesenchymal component is composed of a mixture of spindled cells and collagen fibrils in a loose mucopolysaccharide-rich stroma. Mesenchymal hamartoma in adults is rare. In adults, the tumor tends to contain more hyalinized fibrous tissue and fewer ductal structures and frequently is more vascular than its pediatric counterpart (31).

Infections

Pyogenic Abscess

A hepatic abscess is a localized collection of pus in the liver caused by infectious processes, with destruction of the hepatic parenchyma and stroma. The majority of cases of liver abscess are pyogenic, followed by fungal and amebic. Both pyogenic and amebic abscesses can be multilocular cystic lesions that are composed predominantly of fluid attenuation. More than half of pyogenic liver abscesses are polymicrobic. Common organisms include *Escherichia coli* and species of *Klebsiella*, *Enterococcus*, and *Streptococcus* (34,35).

On a cross-sectional image, the appearance of a pyogenic abscess varies according to the pathologic stage and the pathogen responsible for the infection (36). Multiple clusters of small abscesses may resemble a honeycomb pattern at an early stage of abscess formation (37). After the clusters aggregate and coalesce into a single larger cavity (the cluster sign), a multiseptated large abscess can be observed that shows rim and septa enhancement with a characteristic target appearance (the "double target" sign). The double target consists of a hypoattenuating central pus area that is surrounded by an inner hyperattenuating ring of granulation tissue and an outer hypoattenuating zone of inflammatory edema (Fig 12) (38,39).

Teaching Point

At MR imaging, the characteristic features of these abscesses include intense enhancement of the rim and septa on early gadolinium-enhanced images, which persists with a negligible change in thickness and intensity on later postgadolinium images, and the presence of periabscess increased enhancement on immediate postgadolinium images (Fig 13) (40). Other characteristic signs, including free gas within the lesion and transient hepatic attenuation difference, are helpful in the diagnosis of pyogenic abscess. The central fluid area in a pyogenic abscess reflects the pus cavities caused by liquefaction necrosis of the liver parenchyma. The septa in a pyogenic abscess result from fibrotic tissue with inflammatory infiltrates that consist of epithelioid macrophages, lymphocytes, eosinophils, and neutrophils.

Amebic Abscess

An amebic liver abscess occurs after trophozoites of *Entamoeba histolytica* penetrate the colonic mucosa, enter the portal circulation, and invade the liver parenchyma (41). In amebic abscesses, septation can be observed in 30% of cases. An enhancing and thickened wall with peripheral edema is

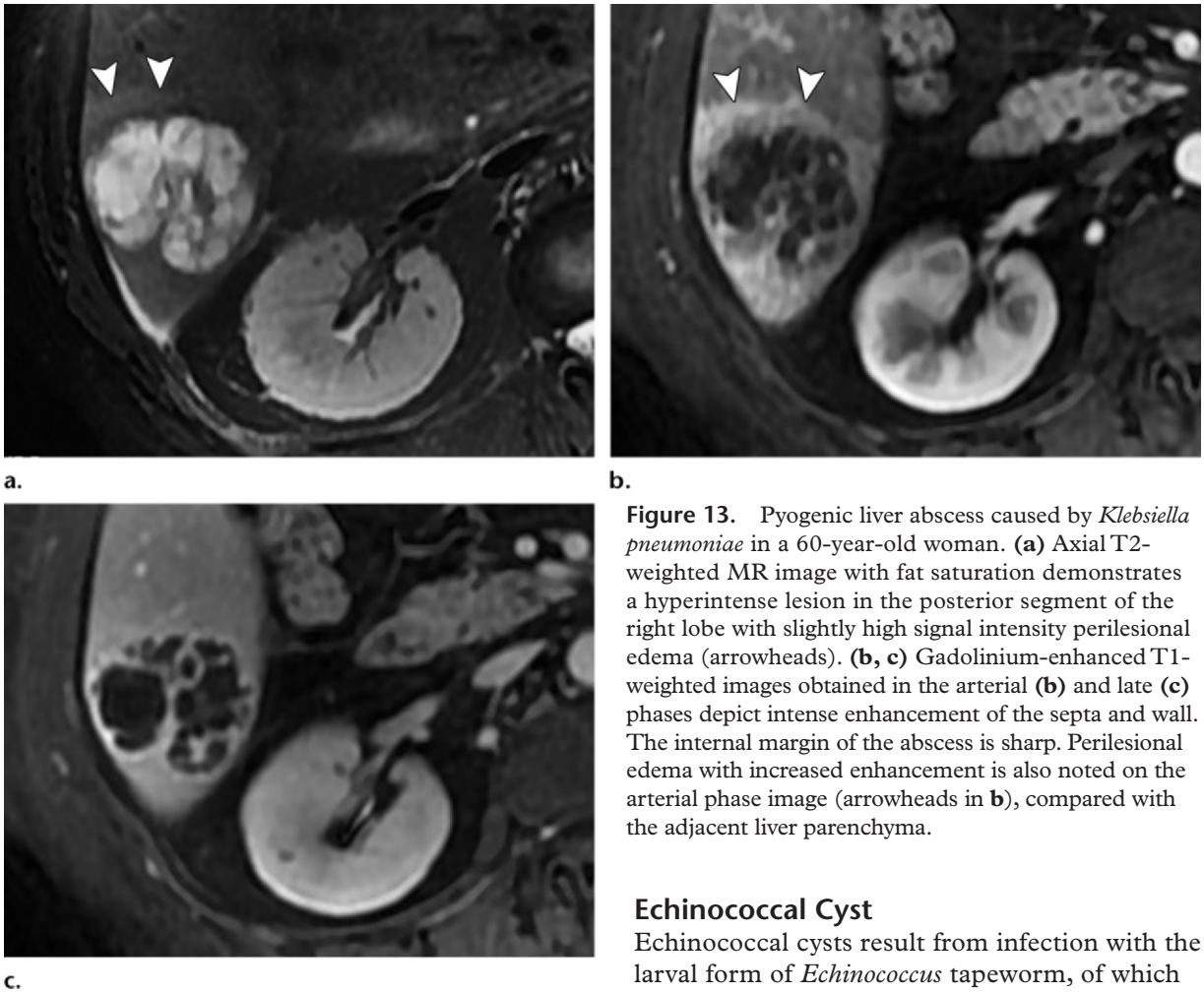

Figure 13. Pyogenic liver abscess caused by *Klebsiella pneumoniae* in a 60-year-old woman. **(a)** Axial T2-weighted MR image with fat saturation demonstrates a hyperintense lesion in the posterior segment of the right lobe with slightly high signal intensity perilesional edema (arrowheads). **(b, c)** Gadolinium-enhanced T1-weighted images obtained in the arterial **(b)** and late **(c)** phases depict intense enhancement of the septa and wall. The internal margin of the abscess is sharp. Perilesional edema with increased enhancement is also noted on the arterial phase image (arrowheads in **b**), compared with the adjacent liver parenchyma.

one of the characteristics, although imaging results are usually indistinct from those of a subacute pyogenic abscess. Differentiation of *E histolytica* largely relies on combining imaging findings with serologic test results. In a septated amebic abscess, the central cystic area is a pus cavity consisting of hemorrhagic granular necrotic material with nuclear debris as well as liquefied liver cells and hemorrhagic, chocolate-colored, pasty material. Septa in an amebic abscess are composed of degenerated liver cells with connective tissue and *E histolytica* trophozoites (42).

The imaging patterns of a multilocular cystic lesion are rarely observed in fungal abscesses. Fungal abscesses can be differentiated from pyogenic or amebic abscesses because the former are typically multiple and small in size (ranging from 2 to 20 mm), whereas the latter are usually solitary and large. Fungal abscesses frequently occur in patients with a compromised immune system, particularly in those with a hematologic malignancy that involves the spleen.

Echinococcal Cyst

Echinococcal cysts result from infection with the larval form of *Echinococcus* tapeworm, of which *Echinococcus granulosis* is the most common type. *Echinococcus multilocularis* is less common but more invasive. Echinococcosis is endemic in many parts of the world, including the Mediterranean region, Africa, South America, the Middle East, Australia, and New Zealand (43). The liver is the most frequently infected organ; the larval oncosphere primarily passes through to the liver by the portal vein after ingestion of contaminated food or water that contains the eggs of the parasite.

Many hepatic echinococcal cysts are asymptomatic and are discovered incidentally at imaging. Large cysts may compress the main bile ducts and hepatic vessels, causing obstructive jaundice or, rarely, portal hypertension. Echinococcal cysts may rupture into the peritoneal cavity, bile duct, pleural cavity, or retroperitoneal space. Leakage of antigen-laden echinococcal cyst fluid into the circulation may result in eosinophilia, anaphylaxis, or even life-threatening anaphylactic shock.

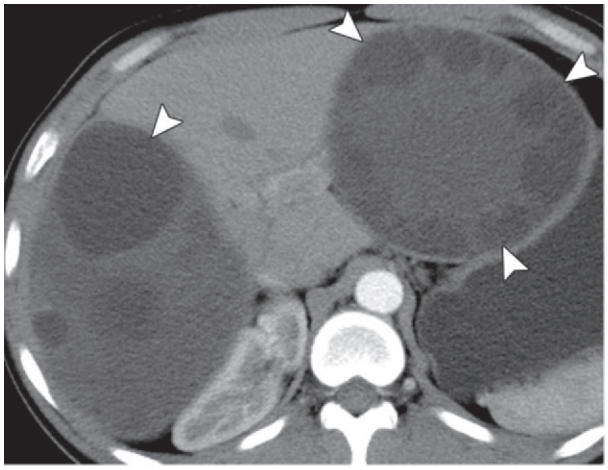

a.

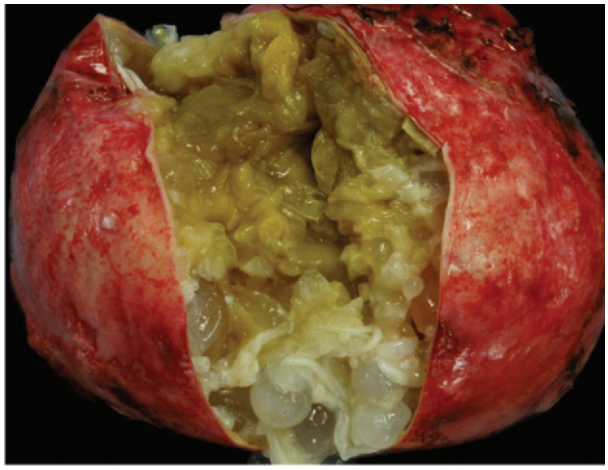

b.

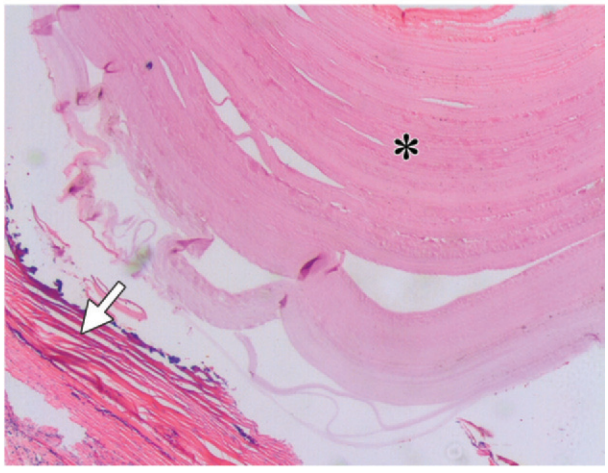

c.

Figure 14. Echinococcal cyst in a 37-year-old Chinese man who lived in an endemic area in western China for 16 years. **(a)** Arterial phase CECT image shows two large, cystic, multilocular lesions with multiple peripherally located daughter cysts (arrowheads). **(b)** Gross pathologic specimen of the lesion in the left hepatic lobe shows a large pericyst containing fluid and numerous daughter cysts of varying sizes. **(c)** Photomicrograph (original magnification, ×40; H-E stain) of the cyst wall depicts the fibrotic pericyst (arrow) with inflammatory and fibrotic tissues and the hyaline laminated layer (*) with a characteristic nonnucleated membrane.

Hepatic echinococcal cysts may be solitary or multiple. A typical echinococcal cyst contains multiple daughter cysts. Radiologic features range from purely cystic lesions with no internal architecture to a complicated heterogeneous mass.

At CT, a mother cyst and peripherally located daughter cysts typically appear as a multilocular cystic lesion with internal septa arranged in a characteristic wheel-spoke pattern (Fig 14a) (43). The average attenuation of mother cysts is usually higher than that of daughter cysts because of debris consisting of hydatid sand and detached cyst walls. Coarse calcifications of the wall are seen in almost half of the cases. Occasionally, thin, linear, floating membranes within the cystic fluid may be observed after the rupture of daughter cysts (44).

At MR imaging, daughter cysts and internal septa are readily visualized on T2-weighted images. Most echinococcal cysts are mixed hypointense on T1-weighted images, depending on the amount of proteinaceous debris, and markedly hyperintense on T2-weighted images. The pericyst appears as a hypointense rim on both T1- and T2-weighted images because of the fibrotic component and the presence of calcifications. Cyst walls and internal septa are enhanced after gadolinium contrast enhancement.

At pathologic examination, hepatic echinococcal cysts consist of three layers. The outer pericyst is derived from the inflammatory and fibrotic tissues of host origin cells that are only a few millimeters thick. The middle laminated layer, called the ectocyst, is a white, acellular membrane that allows nutrient passage. The inner germinal layer is a thin-nucleated membrane that secretes translucent fluid and produces brood capsules by invagination (41).

The brood capsules contain multiple scoleces, namely, embryonic tapeworms, which will develop into daughter cysts after maturation. Daughter cysts replicate the structure of the mother cyst without the pericyst. The cystic fluid contains proteinaceous, translucent, or pale yellow serum transudation. Hydatid sand sediment, which is composed of freed scoleces and detached brood capsules, has also been found in cysts (Fig 14b, 14c) (43).

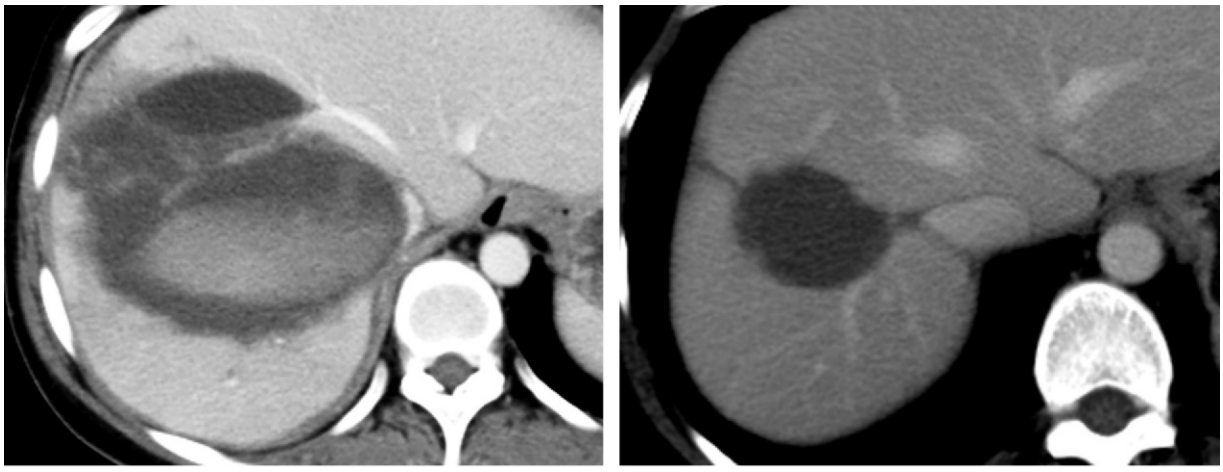

a. b.

Figure 15. Intrahepatic hematoma in a 35-year-old woman. **(a)** Portal venous phase CECT image obtained 10 days after blunt trauma shows a large hematoma with multiple fluid-containing spaces of differing attenuations and coexisting liver lacerations. The patient was treated nonoperatively. **(b)** Follow-up CECT image 8 months later shows contraction of the lesion, with well-defined margins and reduced attenuation (37 HU in the center).

Injuries

Intraparenchymal Hematoma

Hepatic intraparenchymal hematomas may be associated with blunt trauma, surgical procedures, spontaneous hemorrhage in patients with coagulation disorders, syndromic hemolysis with elevated liver enzymes and low platelet count (HELLP syndrome), and rupture of primary hypervascular neoplasms (eg, adenoma, hepatocellular carcinoma, or metastases). CT is useful for identifying parenchymal hematomas and associated findings, including periportal edema, laceration, hemoperitoneum, location of active hemorrhage, and pseudoaneurysm.

At CT, the appearance of an intraparenchymal hematoma depends not only on the cause of the bleeding, elapsed time from the traumatic event, and type of imaging procedure, but also on the mixture percentage of blood, bile, and devascularized tissue debris (36,45). At CECT, acute parenchymal hematomas typically appear as irregular and high-attenuation (40–60 HU) lesions, which represent clotted blood, surrounded by hypoattenuating unclotted blood and bile (Fig 15a). The margin of the hematoma is typically obscured by edema of the surrounding liver parenchyma and microvascular exudation. In the chronic stage, with the degradation of hemoglobin, the hematoma gradually shapes into a well-defined, cystic, low-attenuation fluid collection (Fig 15b).

At MR imaging, subacute hematomas typically appear bright on T1-weighted images due to the T1-shortening effects of methemoglobin. On T1-weighted MR images, chronic hematomas may display a concentric rim sign. The hypointense outer rim results from the deposition of hemosiderin, and the inner hyperintense rim is due to methemoglobin (46). Vague septal structures may occasionally be observed within a hematoma (47). Septa are speculated to reflect the devascularized fragment of less-injured liver tissue as well as the breakdown of blood products and granulation tissue during the healing process.

Biloma

A biloma is an encapsulated collection of bile found after traumatic or iatrogenic injury to the biliary tract. Bilomas typically manifest as well-defined unilocular subcapsular or intrahepatic cystic lesions with water attenuation or signal intensity. A minority of cases are complicated by septa (48). Most locoregional treatment-related bilomas develop within 6 months of the first session of TACE or RFA. The location is subcapsular or close to the ablation zone in RFA, but it can be associated with the arterial territory downstream of the injection site in TACE (49,50).

Bilomas also are associated with hematomas as the delayed complication of blunt trauma. The margin of bilomas is more well defined than that of hematomas. The central attenuation of bilomas (0–15 HU) is lower than that of hematomas. MR imaging can be used to reliably distinguish between pure fluid in a biloma and the blood degeneration products in a hematoma (47). Most

traumatic bilomas may spontaneously regress, but significantly enlarged lesions may cause symptoms or become infected. Enlarged lesions can be treated with percutaneous catheter drainage, which may be combined with endoscopic retrograde cholangiopancreatographic (ERCP) stent placement.

Conclusion

The spectrum of multilocular cystic hepatic lesions includes common and uncommon entities. A lesion's cystic component and internal septa usually reflect its underlying pathologic basis, although imaging findings are not always specific. Familiarity with the patterns and types of these lesions is important in narrowing the list of differential diagnoses.

***Disclosures of Conflicts of Interest*.—J.R.X.:** *Related financial activities:* none. *Other financial activities:* consultant for Bellona Pharmaceutical; expert witness for Science and Technology Bureau, Pudong, Shanghai.

References

1. Morgan DE, Lockhart ME, Canon CL, Holcombe MP, Bynon JS. Polycystic liver disease: multimodality imaging for complications and transplant evaluation. RadioGraphics 2006;26(6):1655–1668.
2. Buetow PC, Buck JL, Pantongrag-Brown L, et al. Biliary cystadenoma and cystadenocarcinoma: clinical-imaging-pathologic correlations with emphasis on the importance of ovarian stroma. Radiology 1995;196(3):805–810.
3. Lam MM, Swanson PE, Upton MP, Yeh MM. Ovarian-type stroma in hepatobiliary cystadenomas and pancreatic mucinous cystic neoplasms: an immunohistochemical study. Am J Clin Pathol 2008; 129(2):211–218.
4. Abdul-Al HM, Makhlouf HR, Goodman ZD. Expression of estrogen and progesterone receptors and inhibin-alpha in hepatobiliary cystadenoma: an immunohistochemical study. Virchows Arch 2007;450 (6):691–697.
5. Korobkin M, Stephens DH, Lee JK, et al. Biliary cystadenoma and cystadenocarcinoma: CT and sonographic findings. AJR Am J Roentgenol 1989;153 (3):507–511.
6. Stevens WR, Gulino SP, Batts KP, Stephens DH, Johnson CD. Mosaic pattern of hepatocellular carcinoma: histologic basis for a characteristic CT appearance. J Comput Assist Tomogr 1996;20(3): 337–342.
7. Jeong YY, Yim NY, Kang HK. Hepatocellular carcinoma in the cirrhotic liver with helical CT and MRI: imaging spectrum and pitfalls of cirrhosis-related nodules. AJR Am J Roentgenol 2005;185(4): 1024–1032.
8. Nino-Murcia M, Olcott EW, Jeffrey RB Jr, Lamm RL, Beaulieu CF, Jain KA. Focal liver lesions: pattern-based classification scheme for enhancement at arterial phase CT. Radiology 2000;215(3):746–751.
9. Silva AC, Evans JM, McCullough AE, Jatoi MA, Vargas HE, Hara AK. MR imaging of hypervascular liver masses: a review of current techniques. RadioGraphics 2009;29(2):385–402.
10. Arrivé L, Fléjou JF, Vilgrain V, et al. Hepatic adenoma: MR findings in 51 pathologically proved lesions. Radiology 1994;193(2):507–512.
11. Ishigami K, Yoshimitsu K, Nishihara Y, et al. Hepatocellular carcinoma with a pseudocapsule on gadolinium-enhanced MR images: correlation with histopathologic findings. Radiology 2009;250(2): 435–443.
12. Bruix J, Sherman M; American Association for the Study of Liver Diseases. Management of hepatocellular carcinoma: an update. Hepatology 2011;53(3): 1020–1022.
13. Kim YS, Rhim H, Lim HK, Choi D, Lee MW, Park MJ. Coagulation necrosis induced by radiofrequency ablation in the liver: histopathologic and radiologic review of usual to extremely rare changes. RadioGraphics 2011;31(2):377–390.
14. Blachar A, Federle MP, Brancatelli G. Hepatic capsular retraction: spectrum of benign and malignant etiologies. Abdom Imaging 2002;27(6):690–699.
15. Danet IM, Semelka RC, Leonardou P, et al. Spectrum of MRI appearances of untreated metastases of the liver. AJR Am J Roentgenol 2003;181(3): 809–817.
16. Kanematsu M, Kondo H, Goshima S, et al. Imaging liver metastases: review and update. Eur J Radiol 2006;58(2):217–228.
17. Warakaulle DR, Gleeson F. MDCT appearance of gastrointestinal stromal tumors after therapy with imatinib mesylate. AJR Am J Roentgenol 2006;186 (2):510–515.
18. Sandrasegaran K, Rajesh A, Rydberg J, Rushing DA, Akisik FM, Henley JD. Gastrointestinal stromal tumors: clinical, radiologic, and pathologic features. AJR Am J Roentgenol 2005;184(3):803–811.
19. Joensuu H. Gastrointestinal stromal tumor (GIST). Ann Oncol 2006;17(suppl 10):x280–x286.
20. Choi D, Yoo EY, Kim KM, et al. Residual and recurrent gastrointestinal stromal tumors with KIT mutations: findings at first follow-up CT after imatinib treatment. AJR Am J Roentgenol 2009;193(2): W100–W105.
21. Suzuki C, Jacobsson H, Hatschek T, et al. Radiologic measurements of tumor response to treatment: practical approaches and limitations. RadioGraphics 2008;28(2):329–344.

22. Hong X, Choi H, Loyer EM, Benjamin RS, Trent JC, Charnsangavej C. Gastrointestinal stromal tumor: role of CT in diagnosis and in response evaluation and surveillance after treatment with imatinib. RadioGraphics 2006;26(2):481–495.
23. Shankar S, vanSonnenberg E, Desai J, Dipiro PJ, Van Den Abbeele A, Demetri GD. Gastrointestinal stromal tumor: new nodule-within-a-mass pattern of recurrence after partial response to imatinib mesylate. Radiology 2005;235(3):892–898.
24. Coffin CM, Fletcher JA. Inflammatory myofibroblastic tumour. In: Fletcher CDM, Unni KK, Mertens F, eds. World Health Organization classification of tumors: pathology and genetics of tumors of soft tissue and bone. Lyon, France: IARC, 2002; 91–93.
25. Yoon KH, Ha HK, Lee JS, et al. Inflammatory pseudotumor of the liver in patients with recurrent pyogenic cholangitis: CT-histopathologic correlation. Radiology 1999;211(2):373–379.
26. Faraj W, Ajouz H, Mukherji D, Kealy G, Shamseddine A, Khalife M. Inflammatory pseudo-tumor of the liver: a rare pathological entity. World J Surg Oncol 2011;9:5.
27. Anderson SW, Kruskal JB, Kane RA. Benign hepatic tumors and iatrogenic pseudotumors. RadioGraphics 2009;29(1):211–229.
28. Fukuya T, Honda H, Matsumata T, et al. Diagnosis of inflammatory pseudotumor of the liver: value of CT. AJR Am J Roentgenol 1994;163(5):1087–1091.
29. Venkataraman S, Semelka RC, Braga L, Danet IM, Woosley JT. Inflammatory myofibroblastic tumor of the hepatobiliary system: report of MR imaging appearance in four patients. Radiology 2003;227(3): 758–763.
30. Kim KA, Kim KW, Park SH, et al. Unusual mesenchymal liver tumors in adults: radiologic-pathologic correlation. AJR Am J Roentgenol 2006;187(5): W481–W489.
31. Stringer MD, Alizai NK. Mesenchymal hamartoma of the liver: a systematic review. J Pediatr Surg 2005;40(11):1681–1690.
32. Goodman ZD, Terracciano LM, Wee A. Tumours and tumour-like lesions of the liver. In: Burt A, Portmann B, Ferrell L, eds. MacSween's pathology of the liver. 6th ed. London, England: Elsevier Health Sciences, 2011; 818–819.
33. Chung EM, Cube R, Lewis RB, Conran RM. Pediatric liver masses: radiologic-pathologic correlation. I. Benign tumors. RadioGraphics 2010;30(3): 801–826.
34. Rahimian J, Wilson T, Oram V, Holzman RS. Pyogenic liver abscess: recent trends in etiology and mortality. Clin Infect Dis 2004;39(11):1654–1659.
35. Alsaif HS, Venkatesh SK, Chan DS, Archuleta S. CT appearance of pyogenic liver abscesses caused by Klebsiella pneumoniae. Radiology 2011;260(1): 129–138.
36. Mortelé KJ, Ros PR. Cystic focal liver lesions in the adult: differential CT and MR imaging features. RadioGraphics 2001;21(4):895–910.
37. Jeffrey RB Jr, Tolentino CS, Chang FC, Federle MP. CT of small pyogenic hepatic abscesses: the cluster sign. AJR Am J Roentgenol 1988;151(3):487–489.
38. Mathieu D, Vasile N, Fagniez PL, Segui S, Grably D, Lardé D. Dynamic CT features of hepatic abscesses. Radiology 1985;154(3):749–752.
39. Murphy BJ, Casillas J, Ros PR, Morillo G, Albores-Saavedra J, Rolfes DB. The CT appearance of cystic masses of the liver. RadioGraphics 1989;9(2): 307–322.
40. Balci NC, Semelka RC, Noone TC, et al. Pyogenic hepatic abscesses: MRI findings on T1- and T2-weighted and serial gadolinium-enhanced gradient-echo images. J Magn Reson Imaging 1999;9(2): 285–290.
41. Mortelé KJ, Segatto E, Ros PR. The infected liver: radiologic-pathologic correlation. RadioGraphics 2004;24(4):937–955.
42. Bhatia R. Intestinal ameoba. In: Bhatia R, ed. Medical parasitology. 2nd ed. New Delhi, India: Jaypee Brothers Publishers, 2002; 37–38.
43. Pedrosa I, Saíz A, Arrazola J, Ferreirós J, Pedrosa CS. Hydatid disease: radiologic and pathologic features and complications. RadioGraphics 2000;20(3): 795–817.
44. Polat P, Kantarci M, Alper F, Suma S, Koruyucu MB, Okur A. Hydatid disease from head to toe. RadioGraphics 2003;23(2):475–494.
45. Savolaine ER, Grecos GP, Howard J, White P. Evolution of CT findings in hepatic hematoma. J Comput Assist Tomogr 1985;9(6):1090–1096.
46. Lee MJ, Hahn PF, Saini S, Mueller PR. Differential diagnosis of hyperintense liver lesions on T1-weighted MR images. AJR Am J Roentgenol 1992; 159(5):1017–1020.
47. Elsayes KM, Narra VR, Yin Y, Mukundan G, Lammle M, Brown JJ. Focal hepatic lesions: diagnostic value of enhancement pattern approach with contrast-enhanced 3D gradient-echo MR imaging. RadioGraphics 2005;25(5):1299–1320.
48. Choudhary N, Duseja A, Kalra N, Chawla Y. Hepatobiliary and pancreatic: intrahepatic biloma after blunt abdominal trauma. J Gastroenterol Hepatol 2011;26(8):1342.
49. Chang IS, Rhim H, Kim SH, et al. Biloma formation after radiofrequency ablation of hepatocellular carcinoma: incidence, imaging features, and clinical significance. AJR Am J Roentgenol 2010;195(5): 1131–1136.
50. Sakamoto I, Iwanaga S, Nagaoki K, et al. Intrahepatic biloma formation (bile duct necrosis) after transcatheter arterial chemoembolization. AJR Am J Roentgenol 2003;181(1):79–87.

Spectrum of Multilocular Cystic Hepatic Lesions: CT and MR Imaging Findings with Pathologic Correlation

Li Jun Qian, MD • Jiong Zhu, MD • Zhi Guo Zhuang, MD • Qiang Xia, MD • Qiang Liu, MD • Jian Rong Xu, MD

RadioGraphics 2013; 33:1419–1433 • **Published online** 10.1148/rg.335125063 • **Content Codes:** CT GI MR

Pages 1419

A cystic lesion is a well-defined lesion with predominant near-water attenuation (0–30 HU) or signal intensity that exhibits negligible enhancement at dynamic imaging; the attenuation or signal intensity can be slightly different from that of pure water because of the diversity in fluid composition.

Page 1420

Generally, the cystic component may be secondary to *(a)* liquid substances, including serous, mucinous, bilious, hemorrhagic, proteinaceous, or mixed fluids; *(b)* intratumoral necrosis; or *(c)* tissue with a high water content. The septa may contain a wide range of tissues, including epithelium, fibrotic tissue, stroma, neoplastic tissue, and inflammatory cells, depending on the lesion type.

Page 1423

The mural nodules in multilocular cystic HCC that correspond to viable tumor components may demonstrate the classic HCC hemodynamics of arterial enhancement and late contrast material washout at both CECT and MR imaging. This feature is critical in differentiating HCC from other cystic neoplasms. Furthermore, if "abnormal internal vessels or a variegated pattern" is observed in mural nodules, it may strongly indicate HCC.

Page 1425

Cystic metastases can be formed through *(a)* necrosis of hypervascular metastases secondary to rapid growth beyond the vascular supply, which is frequently demonstrated in metastases from a neuroendocrine tumor, melanoma, or gastrointestinal stromal tumor (GIST); *(b)* abundant mucin production by acinar structures and glandular tissues from mucinous adenocarcinoma, such as colorectal or ovarian carcinoma; or *(c)* systemic or locoregional treatment

Page 1428

After the clusters aggregate and coalesce into a single larger cavity (the cluster sign), a multiseptated large abscess can be observed that shows rim and septa enhancement with a characteristic target appearance (the "double target" sign). The double target consists of a hypoattenuating central pus area that is surrounded by an inner hyperattenuating ring of granulation tissue and an outer hypoattenuating zone of inflammatory edema.